此計畫成果已經有六篇論文發表，分別列於下:

1. Shu-Pao Wu*, Tzu-Hao Wang, Shi-Rong Liu "A Highly Selective Turn-on Fluorescent Sensor for Copper(II) Ion." *Tetrahedron*, **2010**, *66,* 9655-9658.

2. Shu-Pao Wu*, Yi-Pu Chen, Yi-Ming Sung "Colorimetric Detection of Fe^{3+} Ions Using Pyrophosphate Functionalized Gold Nanoparticles" *Analyst*, **2011**, *136*, 1887-1891.

3. Shi-Rong Liu, Shu-Pao Wu*, "An NBD-based sensitive and selective fluorescent sensor for copper(II) ion**"** *Journal of Fluorescence*, **2011**, *21*, 1599-1605.

4. Shu-Pao Wu*, Zhen-Ming Huang, Shi-Rong Liu, Peter Kun Chung, " A Pyrene-based Highly Selective Turn-on Fluorescent Sensor for Copper(II) Ion and Its Application in Live Cell Imaging" *Journal of Fluorescence*, **2012**, *22*, 253-259.

5. Mani Vedamalai, Shu-Pao Wu*, "A BODIPY-based Highly Selective Fluorescent Chemosensor for Hg^{2+} Ions and its Application to Living Cell Imaging", *European Journal of Organic Chemistry*, **2012**, *6*, 1158-1163.

6. Mani Vedamalai, Shu-Pao Wu*, "A Bodipy-based Colorimetric and Fluorometric Chemosensor for Hg(II) Ions and its Application to Living Cell Imaging", Organic & Biomolecular Chemistry, **2012**, 10, 5410-5416.

第一篇論文 (*Tetrahedron*, **2010**)，化合物2-((pyren-1-yl)methyleneamino)-3-amino maleonitrile可用來偵測Cu(II)，當Cu(II)鍵結時會產生藍色螢光，且對Cu(II)具有高度專一性。
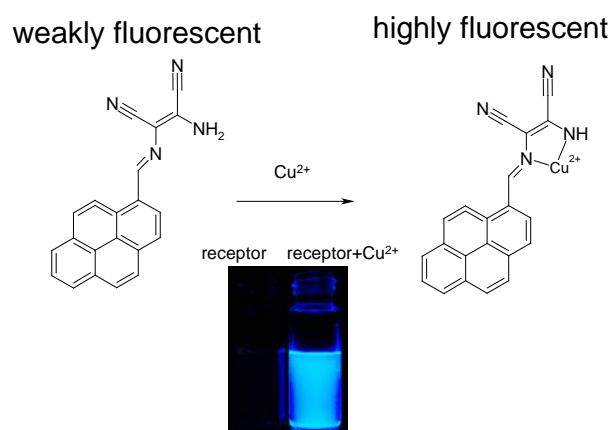

Chemosensor **1** was synthesized through the reaction of diaminomaleonitrile and 1-pyrenealdehyde to form an imine bond between diaminomaleonitrile and pyrene (Scheme 1). Chemosensor **1** is yellow and has an absorption band centered at 421 nm, which is an 86-nm red shift from the typical absorption band of pyrene, 335 nm. Compared to the structure of pyrene, chemosensor **1** has longer conjugated double bonds and its two nitrile groups effectively withdraw electrons. These reasons account for the longer UV-vis absorption wavelength for chemosensor **1** than for pyrene. In addition, chemosensor **1** exhibits weak fluorescence (Φ = 0.0045) compared to pyrene (Φ = 0.6 ~ 0.9). This is due to fluorescence quenching by photoinduced electron

transfer from the lone pair of electrons on the nitrogen atom to pyrene.
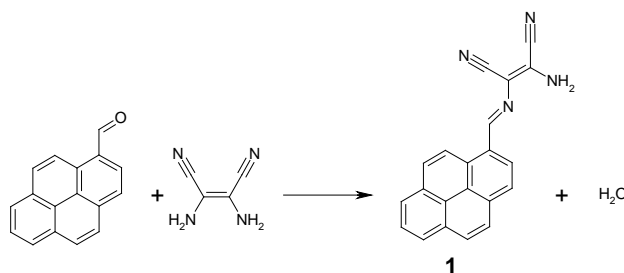
**Scheme 1.** Synthesis of chemosensor **1**

The sensing ability of chemosensor **1** was tested by mixing it with the metal ions Ag^+, Ca^{2+}, Cd^{2+}, Co^{2+}, Cu^{2+}, Fe^{2+}, Fe^{3+}, Hg^{2+}, Mg^{2+}, Mn^{2+}, Ni^{2+}, Pb^{2+} and Zn^{2+}. Cu^{2+} was the only ion that caused a visible color change (from yellow to colorless) and a blue emission from chemosensor **1** (Figure 1). During Cu^{2+} titration with chemosensor **1**, the absorbance at 420 nm decreased and a new band centered at 355 nm was formed. The color change from yellow to colorless (Figure 2) clearly revealed this 65-nm blue shift. The new band centered at 355 nm is close to the absorption band of pyrene, 335 nm. This indicated that Cu^{2+} binding with chemosensor **1** blocked the electron withdrawing ability of the two nitrile groups and resulted in a shorter absorption wavelength.
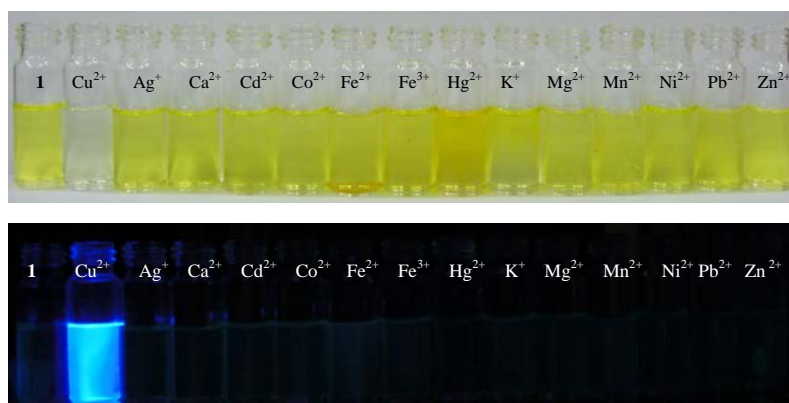

Figure 1. Color (top) and fluorescence (bottom) changes of chemosensor **1** (25 µM) upon addition of various metal ions (100 µM) in acetonitrile-water (v/v = 1:1, 10 mM HEPES, pH = 7.0) solutions
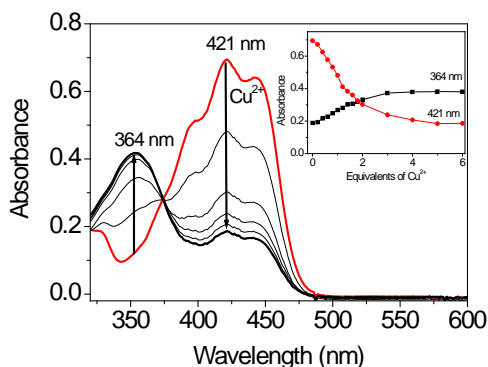
Figure 2. Absorption changes of chemosensor **1** (25 µM) in the presence of various equivalents of Cu^{2+} in acetonitrile-water (v/v = 1:1, 10 mM HEPES, pH = 7.0) solutions

To further evaluate the selectivity of chemosensor **1** toward various metal ions, the fluorescence spectra of chemosensor **1** were taken in the presence of several transition metal ions. However, Cu^{2+} was the only metal ion that caused a significant blue emission (Figure 1). During Cu^{2+} titration with chemosensor **1**, a new emission band centered at 417 nm formed (Figure 3). After adding 4 equivalents of Cu^{2+}, the emission intensity reached a maximum. The quantum yield of the emission band was 0.59, which is 100-fold that of chemosensor **1** at 0.0045. The emission band and quantum yield of chemosensor **1** are similar to the monomer of pyrene, which has a quantum yield of 0.6 ~ 0.9. These observations indicate that Cu^{2+} is the only metal ion that readily binds with chemosensor **1**, causing significant fluorescence enhancement and permitting highly selective detection of Cu^{2+}.
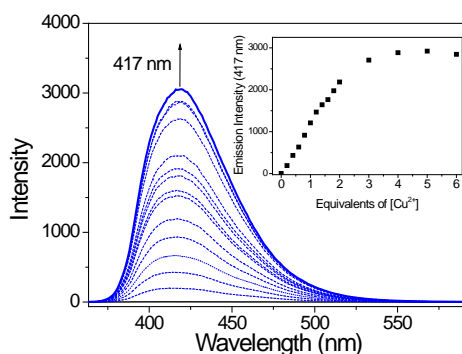

Figure 3. Fluorescence response of chemosensor **1** (25µM) to various equivalents of Cu^{2+} in acetonitrile-water (v/v = 1:1, 10 mM HEPES, pH = 7.0) solutions. The excitation wavelength is 350 nm.

To study the influence of other metal ions on Cu^{2+} binding with chemosensor **1**, this research performed competitive experiments with other metal ions (200 µM) in the presence of Cu^{2+} (100 µM) (Figure 4). Fluorescence enhancement caused by the

mixture of Cu^{2+} with most metal ions was similar to that caused by Cu^{2+} alone. Smaller fluorescence enhancement was observed only when Cu^{2+} was mixed with Fe^{2+} or Fe^{3+} indicating that Fe^{2+} and Fe^{3+} compete with Cu^{2+} for binding with chemosensor **1**. None of the other metal ions was found to interfere with the binding of chemosensor **1** with Cu^{2+}.
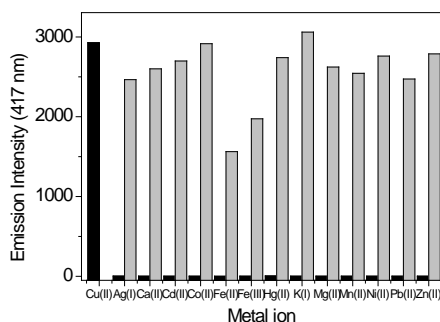
Figure 4. Fluorescence response of chemosensor **1** (25 µM) to Cu^{2+} (100 µM) or 200 µM of other metal ions (the black bar portion) and to the mixture of other metal ions (200 µM) with 100 µM of Cu^{2+} (the gray bar portion) in acetonitrile-water (v/v = 1:1, 10 mM HEPES, pH = 7.0) solutions
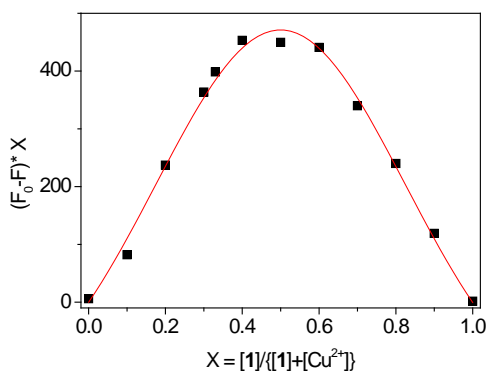
Figure 5. Job plot of the Cu^{2+}-**1** complexes in an acetonitrile-water (v/v = 1:1, 10 mM HEPES, pH = 7.0) solution. The monitored wavelength is 417 nm.

Intercept = $5.21231 *10^{-4}$
Slope = $9.37956*10^{-8}$
$K_a = 5.55*10^3$ M
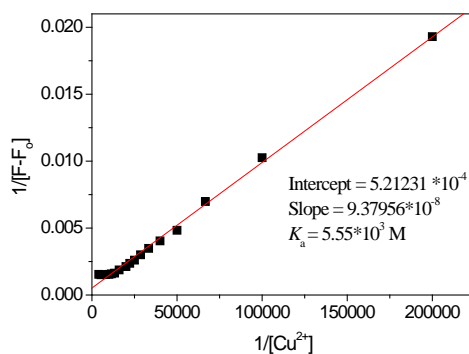
**Figure 6.** Benesi-Hildebrand plot of the Cu^{2+}-**1** complexes in acetonitrile-water (v/v =

1:1 , 10 mM HEPES, pH = 7.0) solutions.

In order to understand the binding stoichiometry of **1**-Cu^{2+} complexes, Job plot experiments were carried out. In Figure 5, the emission intensity at 417 nm is plotted against molar fraction of chemosensor **1** under a constant total concentration. Maximum emission intensity was reached when the molar fraction was 0.5. These results indicate a 1:1 ratio for **1**-Cu^{2+} complexes, in which one Cu^{2+} ion was bound with one chemosensor **1**. The association constant K_a was evaluated graphically by plotting 1/" F against 1/[Cu^{2+}] (Figure 6). The data was linearly fit according to the Benesi–Hilderbrand equation and the K_a value was obtained from the slope and intercept of the line. The apparent association constant (K_a) of Cu^{2+} binding in chemosensor **1** was found to be $5.55*10^3$ M^{-1}.

To gain a clearer understanding of the structure of **1**-Cu^{2+} complexes, ^{1}H NMR and Infrared (IR) spectroscopy were employed. Cu^{2+} is a paramagnetic ion and can affect the proton signals that are close to Cu^{2+} binding site. In the ^{1}H NMR spectra of chemosensor **1**, the proton (NH) signal at 6.4 ppm almost completely disappeared upon the addition of Cu^{2+}. Other peaks remained unchanged. These observations indicated the binding of Cu^{2+} with an amine group. The IR spectra were primarily characterized by bands in the double-bond and triple-bond regions. Two bands, 1628 cm^{-1} and 1598 cm^{-1}, were associated with double bond (C=C and C=N) absorption in chemosensor **1**; two bands, 2232 cm^{-1} and 2204 cm^{-1}, were associated with triple bond (C≡N) absorptions. Binding of Cu^{2+} with chemosensor **1** resulted in a new broad band at 1646 cm^{-1} in the double-bond absorption region; the band at 1598 cm^{-1} remained unchanged. This was due to Cu^{2+}-induced deprotonation of the amine group in chemosensor **1** during Cu^{2+} binding. Cu^{2+}-induced deprotonation of the amine group formed a charge-delocalized species in the five-member chelating ring. This accounts for the formation of a new broad band at 1646 cm^{-1} upon Cu^{2+} binding. In the triple-bond absorption region, two other bands at 2232 cm^{-1} and 2204 cm^{-1} decreased and a new band at 2154 cm^{-1} was observed upon addition of Cu^{2+}. This indicated that the binding of Cu^{2+} with two amine nitrogens in chemosensor **1** affected the electron withdrawing ability of the two nitrile groups and resulted in a shorter wavenumber. According to the result of Job plot, the binding ratio for **1**-Cu^{2+} complexes was 1:1, in which one Cu^{2+} ion was bound with one chemosensor **1**. Cu^{2+} was bound to two nitrogens (Figure 7).
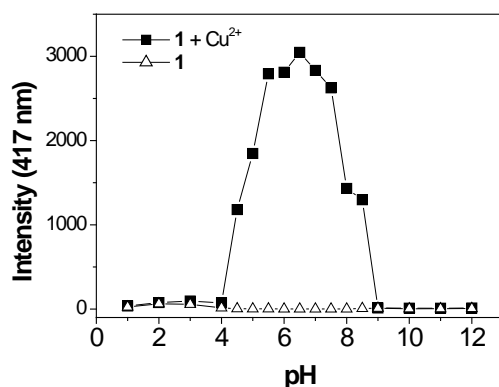
Figure 8. Fluorescence intensity (417 nm) of free chemosensor **1** (25 μM) (△) and after addition of Cu^{2+} (100 μM) (■) in an acetonitrile-water (v/v = 1/1, 10 mM buffer) solution as a function of different pH values. The excitation wavelength was 350 nm.

    The study performed pH titration of chemosensor **1** to investigate a suitable pH range for Cu^{2+} sensing. As depicted in Figure 8, the emission intensities of metal-free chemosensor **1** were very low. After mixing chemosensor **1** with Cu^{2+}, the emission intensity at 417 nm suddenly increased at pH 5.0 and reached a maximum in the pH range of 5.5 to 7.5. When pH exceeded higher than 8.5, the emission intensity dropped sharply to zero. This indicates poor stability of the **1**-Cu^{2+} complexes at high pH. For pH < 5, the emission intensity is very low due to the protonation of the amine groups that prevents the formation of **1**-Cu^{2+} complexes.

Conclusion

    In conclusion, this study developed a pyrene-based fluorescent chemosensor for Cu^{2+} sensing. The experiment synthesized chemosensor **1** from the reaction of diaminomaleonitrile and 1-pyrenealdehyde to form an imine bond between diaminomaleonitrile and pyrene. We observe significant fluorescence enhancement with chemosensor **1** in the presence of Cu^{2+}. However, adding Ag^+, Ca^{2+}, Cd^{2+}, Co^{2+}, Fe^{2+}, Fe^{3+}, Hg^{2+}, Mg^{2+}, Mn^{2+}, Ni^{2+}, Pb^{2+}, or Zn^{2+} to the chemosensor solution caused only minimal change in fluorescence emission. The optimal pH range for Cu^{2+} detection by chemosensor **1** is 5 ~ 7.5. This pyrene-based Cu^{2+} chemosensor provides an effective means of Cu^{2+} sensing.

第二篇論文（*Analyst*, **2011**），使用表面修飾焦磷酸根的奈米金粒子，來偵測 $Fe(III)$ 離子；$Fe(III)$ 會使得焦磷酸根的奈米金粒子產生聚集，奈米金粒子的顏色由深紅色變為藍色，此方法可應用於環境中 $Fe(III)$ 離子的偵測。
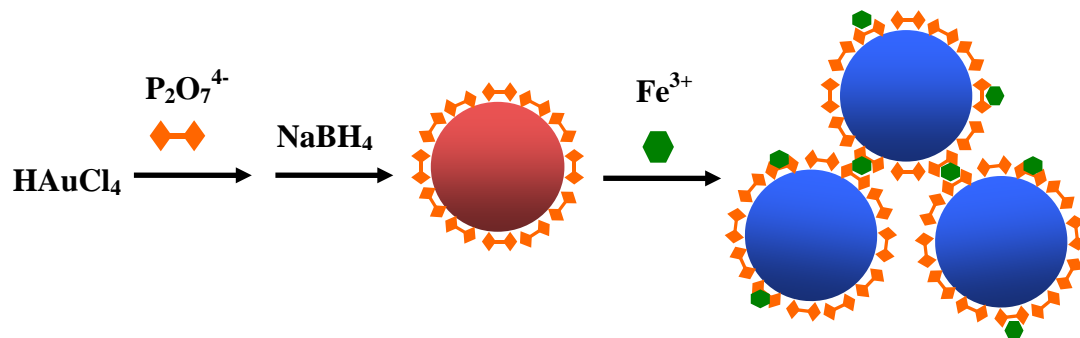

The Characterization of $P_2O_7^{4-}$-AuNPs

TEM images revealed that $P_2O_7^{4-}$-AuNP sizes ranged from 16 to 70 nm, with most particles size falling in the range 26 ~ 30 nm (Figure 1). The $P_2O_7^{4-}$-AuNPs were also characterized using IR spectroscopy. The strong peaks at 929 cm^{-1} and 1117 cm^{-1} were assigned to P-O stretches in pyrophosphate. When pyrophosphate was modified on the surface of the Au nanoparticles, only one broad peak was observed at 1090 cm^{-1}; this is evidence for the existence of $P_2O_7^{4-}$-AuNPs. The SPR absorption of AuNPs was measured using a UV-vis spectrophotometer. The particle concentration of the AuNPs (~ 0.5 nM) was determined according to Beer's law, using an extinction coefficient of ~10^9 M^{-1}cm^{-1} at 535 nm for the AuNPs.
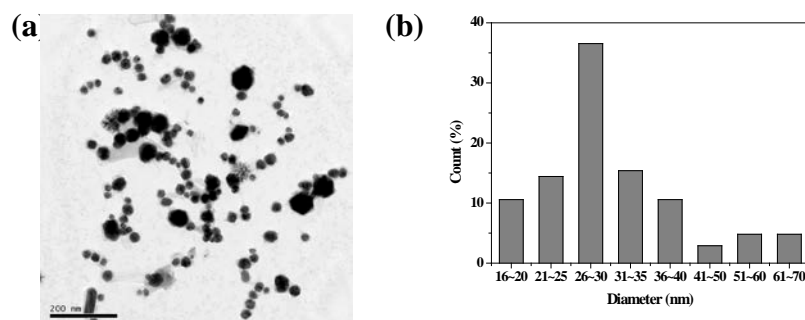
Figure 1. (a) TEM images of $P_2O_7^{4-}$-AuNPs. The scale bar for TEM images is 200 nm. (b) The size distribution of $P_2O_7^{4-}$-AuNPs.
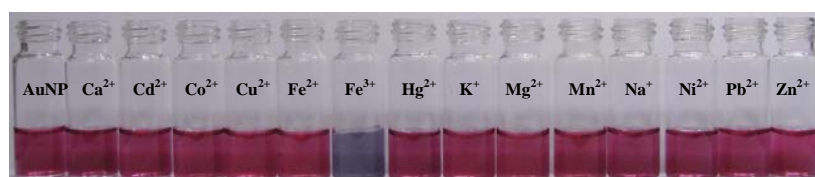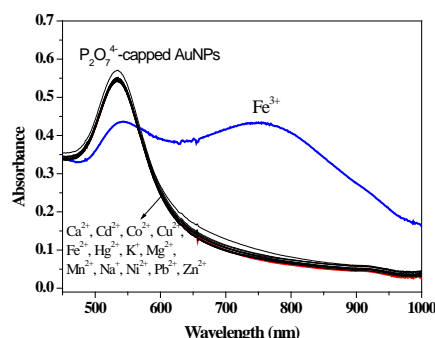
Figure 2. (Top) Photographic images of $P_2O_7^{4-}$-AuNPs in the present of various metal ions. (Bottom) UV-vis spectra of $P_2O_7^{4-}$-AuNPs in the presence of different metal ions (150 μM). Buffer: [Hepes] = 10 mM, pH 7.

## Interaction of $P_2O_7^{4-}$-AuNPs with various Metal Ions

Firstly, the bonding capability of $P_2O_7^{4-}$-AuNPs with metal ions as a measure of the applicability of colorimetric detection in aqueous solutions was tested. To evaluate the selectivity of $P_2O_7^{4-}$-AuNPs towards various metal ions, the absorption spectra of $P_2O_7^{4-}$-AuNPs were taken in the presence of several metal ions: Ca^{2+}, Cd^{2+}, Co^{2+}, Cu^{2+}, Fe^{2+}, Fe^{3+}, Hg^{2+}, K^+, Mg^{2+}, Mn^{2+}, Na^+, Ni^{2+}, Pb^{2+}, and Zn^{2+}. Figure 2 shows the effect of metal ions on the appearance of $P_2O_7^{4-}$-AuNPs in solution. Fe^{3+} was the only ion which resulted in an absorption peak shift from 535 nm to 750 nm. This red shift was also observed as a color change from pink to blue. Other metal ions did not influence the absorption spectra, indicating that no aggregation occurred.

Fe^{3+} triggered aggregation of $P_2O_7^{4-}$-AuNPs was mainly through two-step binding. The first step involves pyrophosphate binding to a Fe^{3+} ion through two oxygens. Secondly, bonds formed between Fe^{3+} and oxygen atoms in another pyrophosphate capped onto adjacent AuNPs resulting in aggregation. Figure 3 shows the TEM image of Fe^{3+} induced aggregation of $P_2O_7^{4-}$-AuNPs. Effectively, Fe^{3+} functioned as a bridge between particles, and triggered the aggregation of $P_2O_7^{4-}$-AuNPs.

The degree of aggregation of $P_2O_7^{4-}$-AuNPs depended on the concentration of Fe^{3+} ions; Figure 4 shows the SPR absorption change with the addition of different concentrations of Fe^{3+}. The absorbance at 535 nm decreased with increasing Fe^{3+} concentration. A new band at 750 nm was formed during Fe^{3+} titration as a result of the induced aggregation of AuNPs. A linear relationship was found when the concentration of Fe^{3+} ions was between 10 μM and 60 μM. The limit of detection for Fe^{3+} was found to be 5.6 μM.
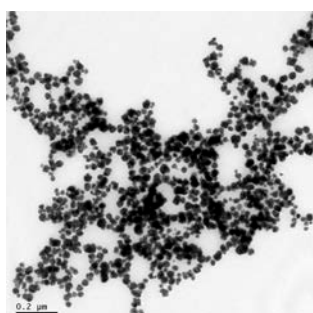
Figure 3. TEM images of $P_2O_7^{4-}$-AuNPs in the presence of Fe^{3+} ions (150 µM). Buffer: [Hepes] = 10 mM, pH 7.
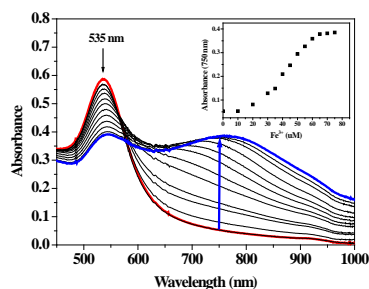

Figure 4. Surface plasmon resonance absorption change of $P_2O_7^{4-}$-AuNPs in the presence of different concentrations of Fe^{3+}. Buffer: [Hepes] = 10 mM, pH 7.
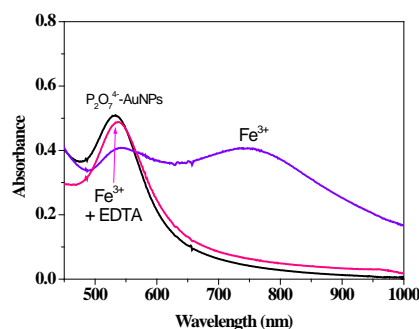
Figure 5. Reversible binding of Fe^{3+} with $P_2O_7^{4-}$-AuNPs. The black line is the UV-vis spectra of $P_2O_7^{4-}$-AuNPs. The blue line is the UV-vis spectra of $P_2O_7^{4-}$-AuNPs in the presence of Fe^{3+} (75 µM). The red line is the UV-vis spectra of $P_2O_7^{4-}$-AuNPs in the presence of Fe^{3+} (75 µM) followed by addition of EDTA (150 µM). Buffer: [Hepes] = 10 mM, pH 7.

Aggregated $P_2O_7^{4-}$-AuNPs can be redispersed by removing Fe^{3+} ions with EDTA; this was confirmed by the consequent SPR absorption shift from 750 nm to 535 nm (Figure 5). After removing the solution using a centrifuge and suspending with an aqueous media, the dispersed $P_2O_7^{4-}$-AuNPs can be reused to detect Fe^{3+}. Through this technique, the $P_2O_7^{4-}$-AuNPs system can be used repeatedly for the detection of Fe^{3+}.
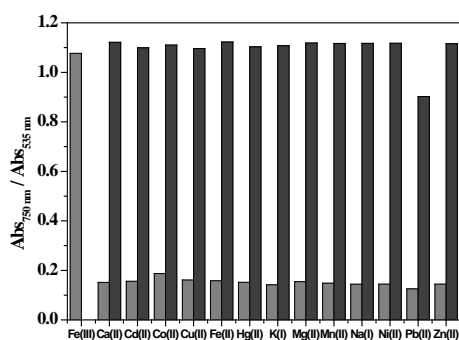
Figure 6. Absorbance ratio ($A_{750\ nm}/A_{535\ nm}$) upon the addition of $P_2O_7^{4-}$-AuNPs to Fe^{3+} for the selected metal ions. Gray bars represent the addition of single metal ion (75 μM); black bars are the addition of Fe^{3+} (75 μM) with another metal ion (300 μM). Buffer: [Hepes] = 10 mM, pH 7.

Interference Studies

In order to study the influence of other metal ions on Fe^{3+} binding to $P_2O_7^{4-}$-AuNPs, competitive experiments were carried out in the presence of Fe^{3+} (75 μM) with Ca^{2+}, Cd^{2+}, Co^{2+}, Cu^{2+}, Fe^{2+}, Fe^{3+}, Hg^{2+}, K^+, Mg^{2+}, Mn^{2+}, Na^+, Ni^{2+}, Pb^{2+}, and Zn^{2+} at 150 μM (Figure 6). The SPR absorption shift caused by the mixture of Fe^{3+} with the other metal ion was similar to that caused solely by Fe^{3+}. This indicates that other metal ions did not interfere in the binding of $P_2O_7^{4-}$-AuNPs with Fe^{3+}. This finding is consistent with previous studies suggesting that Fe^{3+} is the only metal ion that can be bound to the $P_2O_7^{4-}$-AuNPs.

The Influence of pH on Fe^{3+}-induced Aggregation of $P_2O_7^{4-}$-AuNPs

To investigate the pH range in which $P_2O_7^{4-}$-AuNPs can effectively detect Fe^{3+}, a pH titration of $P_2O_7^{4-}$-AuNPs was carried out. Figure 7 shows that the absorbance ratio (A_{750}/A_{535}) of $P_2O_7^{4-}$-AuNPs increased when the pH values were less than 2.5. Thus, under acidic conditions (pH < 2.5), protonation of pyrophosphate resulted in the aggregation of AuNPs. In the pH range of 3 to 12, the absorbance ratio (A_{750}/A_{535}) was constant. This indicates that $P_2O_7^{4-}$-AuNPs were stable in the pH range of 3 to 12. The influence of pH on Fe^{3+}-induced aggregation of $P_2O_7^{4-}$-AuNPs is shown in Figure 7; addition of Fe^{3+} resulted in a high absorbance ratio (A_{750}/A_{535}) in a pH range of 3 to 9. At pH > 9, the absorbance ratio (A_{750}/A_{535}) decreased due to the formation of $Fe(OH)_3$ colloidal. Under acidic conditions (pH < 2.5), the absorbance ratios ($A_{750\ nm}/A_{535\ nm}$) in the presence of Fe^{3+} were slightly higher than without Fe^{3+}. The acidic conditions (pH < 2.5) caused the aggregation of $P_2O_7^{4-}$-AuNPs and as a result these conditions were found to be unsuitable for monitoring Fe^{3+} by means of SPR absorption change.
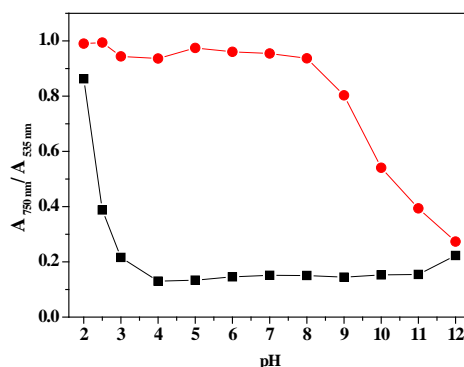
Figure 7. Influence of pH on the UV/vis spectra of $P_2O_7^{4-}$-AuNPs in the absence ( ) and presence (Ϊ) of Fe^{3+} (150 μM). The buffers (10 mM) were: pH 1 ~ 2, KCl/HCl; pH 2.5 ~ 4, KH_2PO_4/HCl; pH 4.5 ~ 6, KH_2PO_4/NaOH; pH 6.5 ~ 10, Hepes; pH 10 ~ 12, Tris-HCl.

Application of $P_2O_7^{4-}$-AuNPs for the Analysis of Lake Water Samples

To confirm the practical application of $P_2O_7^{4-}$-AuNPs, water samples from different lakes located in Hsinchu, Taiwan, were collected. All water samples were filtered through a 0.2 μm membrane and then analyzed using ICP-AES. A calibration curve of $P_2O_7^{4-}$-AuNPs SPR shifts in the presence of different concentrations of Fe^{3+} was prepared. The analytical results are shown in Table 1. The results obtained with $P_2O_7^{4-}$-AuNPs were in good agreement with those obtained using the ICP-AES method, with a relative error of less than 9 %. These results demonstrate that the designed probe is applicable for Fe^{3+} detection in water samples.

**Table 1**. Results of Fe^{3+} detection in lake water samples

	ICP-AES	proposed method[a]	relative error (%)
sample 1	$(25.61\pm0.09) \times 10^{-6}$ M	$(26.60\pm0.11) \times 10^{-6}$ M	3.72
sample 2	$(21.31\pm0.10) \times 10^{-6}$ M	$(22.34\pm0.10) \times 10^{-6}$ M	4.61
sample 3	$(14.25\pm0.08) \times 10^{-6}$ M	$(15.56\pm0.08) \times 10^{-6}$ M	8.41

[a] using $P_2O_7^{4-}$-capped AuNPs.

Conclusion

This report demonstrated that pyrophosphate-capped AuNPs can be used to effectively detect Fe^{3+} ions. Fe^{3+} was the only metal ion which induced aggregation of $P_2O_7^{4-}$-AuNPs resulting in a color change from pink to blue, and a corresponding SPR absorption shift from 535 nm to 750 nm. The optimal pH range for Fe^{3+} detection using $P_2O_7^{4-}$-AuNPs was determined to be from 3 to 9.

第三篇論文（*Journal of Fluorescence*, **2011**），合成以NBD 化合物可用來偵測Cu(II)，當Cu(II)鍵結時會產生黃色螢光淬息，且對Cu(II)具有高度專一性。
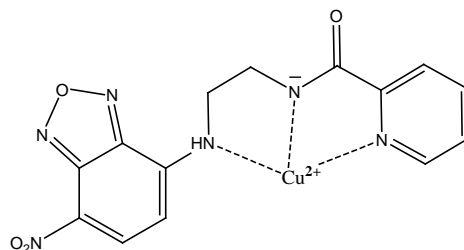
Synthesis of chemosensor 1

Chemosensor **1** comprises two parts: an NBD moiety and *N*-(2-aminoethyl)picolinamide. Reaction of picolinoyl chloride with *tert*-butyl 2-aminoethylcarbamate in equimolar quantities, and deprotection with trifluoroacetic acid (TFA),furnished the chelator *N*-(2-aminoethyl)-picolinamide. The reaction of *N*-(2-aminoethyl)picolinamide with NBD-Cl provided Chemosensor **1** (Scheme 1). Chemosensor **1** is yellow, with an absorption band centered at 472 nm, and the sensor exhibits a green emission band centered on 544 nm with quantum yield, $\Phi = 0.03$.
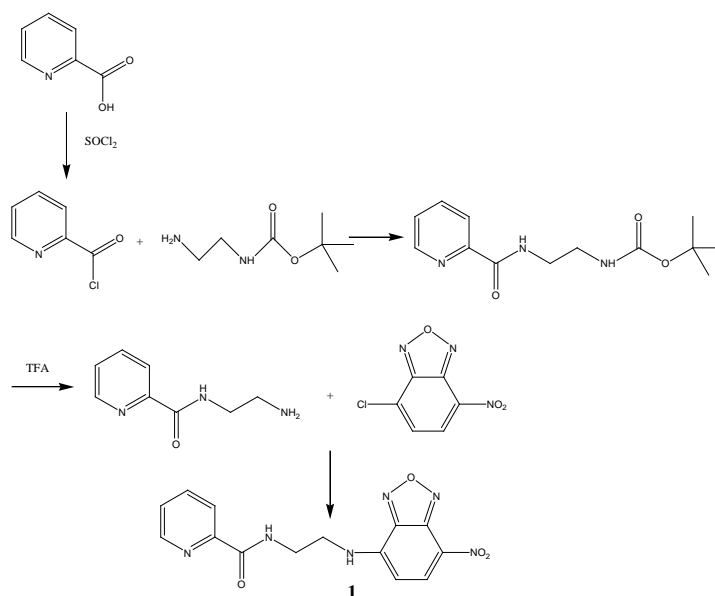

Scheme 1. Synthesis of chemosensor **1**

Cation-sensing properties

We tested the sensing ability of chemosensor **1** by mixing it with the metal ions Ca^{2+}, Cd^{2+}, Co^{2+}, Cu^{2+}, Fe^{2+}, Hg^{2+}, Mg^{2+}, Mn^{2+}, Ni^{2+} and Zn^{2+}. Figure 1 shows that

addition of most metal ions did not cause a change in intensity; Cu^{2+} was the only ion that caused significant fluorescent quenching in chemosensor **1**. Upon binding with Cu^{2+}, the sensors green emission was completely quenched (Figure 2). During Cu^{2+} titration with chemosensor **1**, the intensity of the 544 m emission band decreased (Figure 3). After addition of greater than one molar equivalent of Cu^{2+}, the emission intensity reached a minimum. These observations suggest that Cu^{2+} is the only metal ion that readily binds with chemosensor **1**, causing significant fluorescence quenching, and permitting highly selective detection of Cu^{2+}.
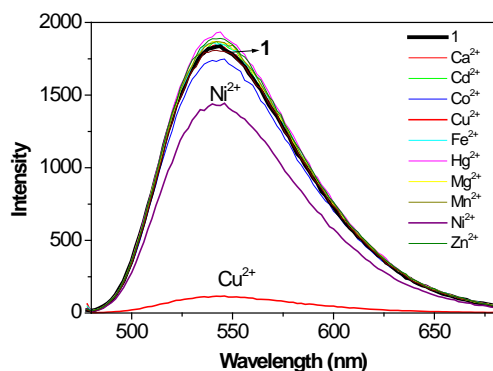
Figure 1. Fluorescence response of chemosensor **1** (100 µM) to different metal ions (1 mM) in a methanol-water (v/v = 1/1, 10 mM Hepes buffer, pH 7.0) solution.

To study the influence of other metal ions on Cu^{2+} binding with chemosensor **1**, we performed competitive experiments with other metal ions (100 µM) in the presence of Cu^{2+} (100 µM) (Figure 4). Fluorescence quenching caused by the Cu^{2+} solution with most metal ions was similar to that caused by Cu^{2+} alone. This indicated that the other metal ions did not interfere significantly with the binding of chemosensor **1** with Cu^{2+}.
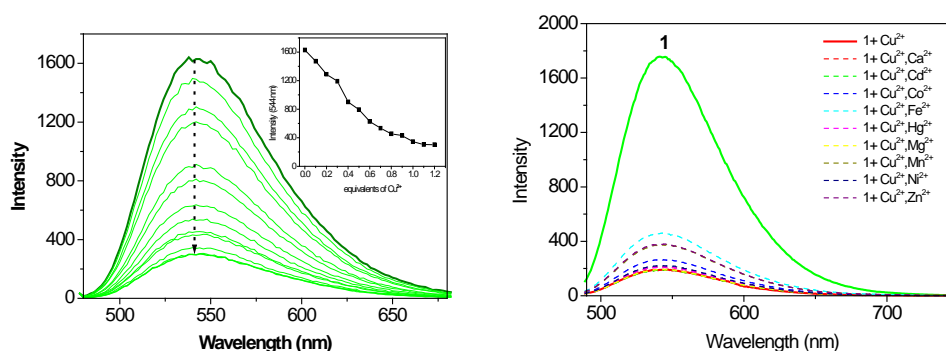

(Right) **Figure 3.** Fluorescence response of chemosensor **1** (100 µM) with various Cu^{2+} ion concentrations, in a methanol-water (v/v = 1/1, 10 mM Hepes buffer, pH 7.0) solution. (Left) **Figure 4.** Fluorescent response of **1** (100 µM) to Cu^{2+} (100 µM) over the selected metal ions (100 µM). All spectra were taken at 25 ^{0}C in a methanol-water

(v/v = 1/1, 10 mM Hepes buffer, pH 7.0) solution at excitation wavelength 473 nm.

In order to understand the binding stoichiometry of Chemosensor **1**-Cu^{2+} complexes, we carried out a series of Job plot experiments. Figure 5 plots the emission intensity at 544 nm against chemosensor **1** molar fraction, under a constant total concentration of **1**. Maximum fluorescent quenching occurred for a 0.5 mole fraction. This result indicates a 1:1 ratio for **1**-Cu^{2+} complexes, in which one Cu^{2+} ion binds with one chemosensor **1**. Evaluating the association constant, K_a, graphically by plotting $1/"F$ against $1/[Cu^{2+}]$ produces Figure 6. Linearly fitting the data to the Benesi–Hilderbrand equation, allows K_a to be determined from the slope and intercept of the plot. The apparent association constant, K_a, for Cu^{2+} binding in chemosensor **1** was determined as $1.22 \times 10^3 \, M^{-1}$. The detection limit of chemosensor **1** as a fluorescent sensor for the analysis of Cu^{2+} was determined from the plot of fluorescence intensity as a function of the concentration of Cu^{2+} (Figure 7). It was found that chemosensor **1** has a detection limit of 9.6 µM, which is allowed for the detection of micromolar concentration range of Cu^{2+}.
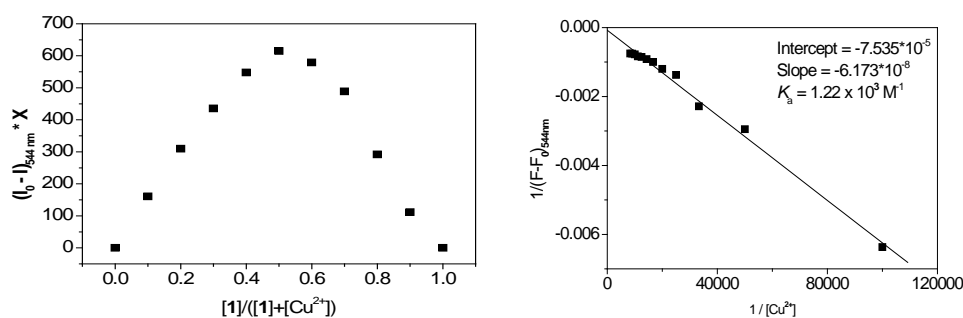

(Left) **Figure 5.** Job plot of a 1:1 complex of **1**-Cu^{2+}, where the 544 nm emission is plotted against mole fraction of chemosensor **1,** at a constant total concentration of $2.0*10^{-4}$ M in a methanol-water (v/v = 1/1, 10 mM Hepes buffer, pH 7.0) solution. (Right) **Figure 6.** Benesi-Hilderbrand plot of **1** with $Cu(BF_4)_2$.
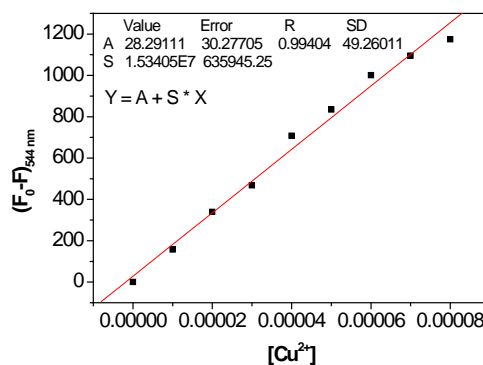
Figure 7. Calibration curve of Cu^{2+}-**1** (100 µM) in a methanol-water (v/v = 1/1, 10 mM Hepes buffer, pH 7.0). The excitation wavelength was 473 nm, and the monitored

emission wavelength was 544 nm. The detection limit (DL) of Cu^{2+} ions using chemosensor **1** was determined from the following equation: DL = K * SD / S, where K = 3; SD is the standard deviation of the blank solution; S is the slope of the calibration curve. DL = K * SD / S = 3 * 49.26011 / $1.53405*10^7$ = $9.6*10^{-6}$ M (9.6 μM)

To gain a clearer understanding of the structure of **1**-Cu^{2+} complexes, ^{1}H NMR and Infrared (IR) spectroscopy were employed. Cu^{2+} is a paramagnetic ion and can affect the proton signals that are close to Cu^{2+} binding site. In the ^{1}H NMR spectra of chemosensor **1** (Figure 8), adding Cu^{2+} caused the proton (amide NH) signal at 9.2 ppm and the proton (at pyridine) signals at 7.6, 8.0, 8.65 ppm to almost completely disappear. Other peaks (protons at NBD) at 6.5, 8.5 ppm became broad upon Cu^{2+} addition. These observations indicated the binding of Cu^{2+} with an amide group, pyridine and an amine attached to the NBD motif. The IR spectra were primarily characterized by bands in the double-bond region (Figure 9). The band 1633 cm^{-1} was associated with double-bond (C=O) absorption in chemosensor **1**. Binding of Cu^{2+} with chemosensor **1** resulted in a shift from 1633 cm^{-1} to 1629 cm^{-1} in the double-bond absorption region, due to the amide group in chemosensor **1**. The Job plot indicates that the binding ratio for chemosensor **1**-Cu^{2+} complexes was 1:1. Cu^{2+} was bound to one nitrogen atom from pyridine, one nitrogen atom from amide and one nitrogen atom attached to the NBD motif (Figure 10).
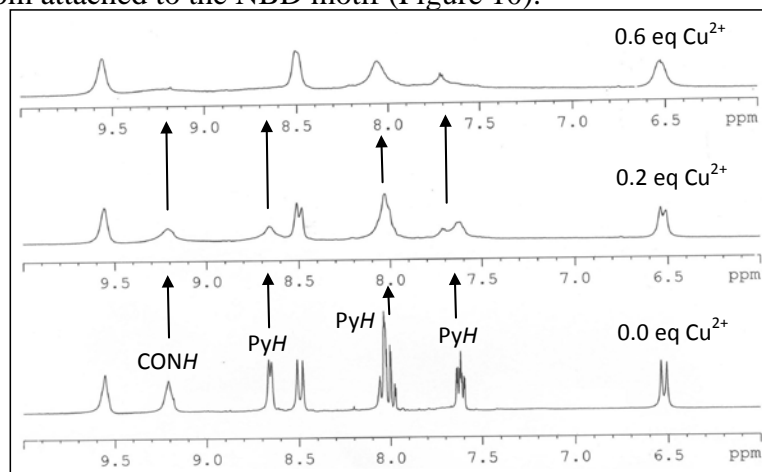
Figure 8. ^{1}H NMR spectra of chemosensor **1** (5 mM) in the presence of different amount of Cu^{2+} in DMSO-d_6.

We performed pH titration of chemosensor **1** to investigate a suitable pH range for Cu^{2+} sensing. As depicted in Figure 11, the emission intensities of metal-free chemosensor **1** remained unchanged. Only when pH was less than 3, did intensity slightly decreased. This was due to protonation of the bridging amine nitrogen, which bonds to NBD. In the presence of Cu^{2+}, the emission intensity at 544 nm suddenly decreased at pH 5.0 and reached lowest intensity in the range of pH 6 to pH 10. This

indicates the formation of the 1-Cu^{2+} complex at high pH values. This observation also reveals that the formation of the 1-Cu^{2+} complexes is a deprotonation process (Figure 10). Cu^{2+} binding induced protonation of the amide in chemosensor 1. For pH < 5, the emission intensity remained higher due to the protonation of the amine groups, preventing the formation of 1-Cu^{2+} complexes.
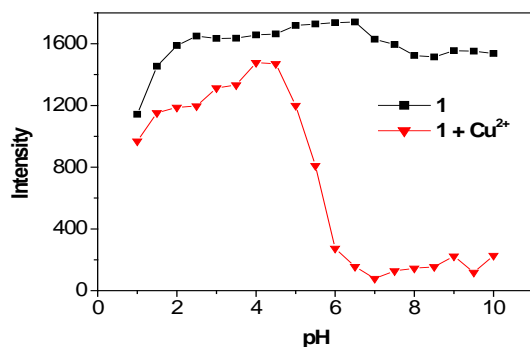

Figure 11. Influence of pH on the fluorescence spectra for 1 (100 µM) both when pure, and in combination with Cu^{2+} (100 µM).

Conclusion

In conclusion, this study developed a NBD-based fluorescent chemosensor for Cu^{2+} ion sensing. We synthesized chemosensor 1 from the reaction of N-(2-aminoethyl)picolinamide and NBD-Cl, to form a new C-N bond between the two precursors. We observed significant fluorescence quenching with chemosensor 1 in the presence of Cu^{2+} ion, while, adding Ca^{2+}, Cd^{2+}, Co^{2+}, Fe^{2+}, Hg^{2+}, Mg^{2+}, Mn^{2+}, Ni^{2+}, or Zn^{2+} to the chemosensor solution caused only minimal changes in fluorescence emission intensity. The optimal pH range for Cu^{2+} detection by chemosensor 1 was pH 6 – 10. This NBD-based Cu^{2+} chemosensor provides an effective, and non-destructive means of Cu^{2+} ion sensing.

第四篇論文（*Journal of Fluorescence*, **2012**），合成以pyrene 化合物可用來偵測Cu(II)，當Cu(II)鍵結時會產生藍色螢光，且對Cu(II)具有高度專一性。
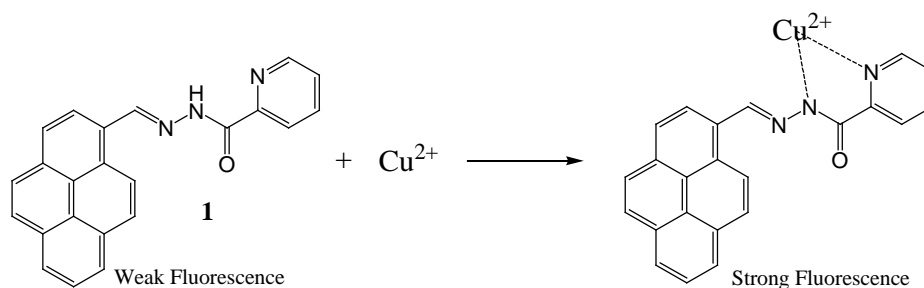
Spectral Characteristics of Chemosensor **1**

The synthesis of chemosensor **1** consisted of two steps (scheme 1): the formation of 1-pyrenecarboxaldehyde hydrazone and its further reaction with picolinoyl chloride. Chemosensor **1** is colorless and has an absorption band centered at 360 nm, which is near the typical absorption band of pyrene, 335 nm [28]. In addition, chemosensor **1** exhibits weaker fluorescence (Φ = 0.013) than does pyrene (Φ = 0.6 ~ 0.9) [29]. This is due to fluorescence quenching by PET from the lone pair of electrons on the nitrogen atom to pyrene.

Cation-sensing Properties
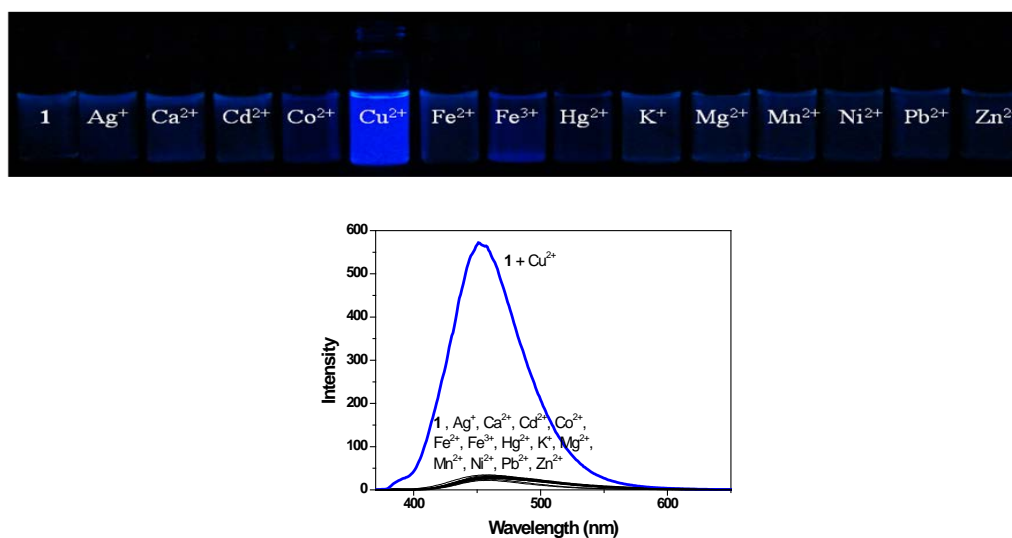
Figure 1. Fluorescence emission (top) and spectra (bottom) of chemosensor **1** (25 µM) upon addition of various metal ions (50 µM) in methanol-water (v/v = 7:3, 6 mM HEPES, pH 7.0) solutions. The excitation wavelength was 360 nm.

The sensing ability of chemosensor **1** was tested by mixing it with the metal ions Ag^+, Ca^{2+}, Cd^{2+}, Co^{2+}, Cu^{2+}, Fe^{2+}, Fe^{3+}, Hg^{2+}, K^+, Mg^{2+}, Mn^{2+}, Ni^{2+}, Pb^{2+}, and Zn^{2+}. To further evaluate the selectivity of chemosensor **1** toward various metal ions, the fluorescence spectra of chemosensor **1** were taken in the presence of several transition metal ions. Cu^{2+} was the only metal ion that caused a significant blue emission

(Figure 1). During Cu^{2+} titration with chemosensor **1**, a new emission band centered at 455 nm formed (Figure 2). After adding two equivalents of Cu^{2+}, the emission intensity reached a maximum. The quantum yield of that emission band was 0.267, which is 20-fold that of chemosensor **1,** 0.013. These observations indicate that Cu^{2+} is the only metal ion that readily binds with chemosensor **1**, significantly enhancing fluorescence and permitting highly selective detection of Cu^{2+}.
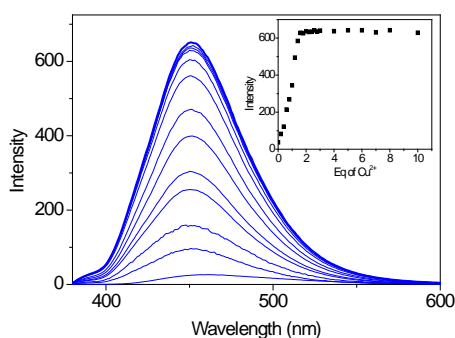
Figure 2. Fluorescence response of chemosensor **1** (25 µM) to various equivalents of Cu^{2+} in methanol-water (v/v = 7:3, 6 mM HEPES, pH 7.0) solutions. The excitation wavelength was 360 nm.

To study the influence of other metal ions on Cu^{2+} binding with chemosensor **1**, this research tested Cu^{2+} (100 µM) in combination with each of the other metal ions (100 µM) (Figure 3). Fluorescence enhancement caused by the mixture of Cu^{2+} with most metal ions was similar to that caused by Cu^{2+} alone. This observation indicates that most of the other metal ions did not interfere with the binding of chemosensor **1** with Cu^{2+}.
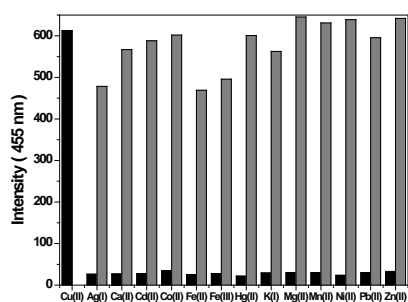

Figure 3. Fluorescence response of chemosensor **1** (25 µM) to Cu^{2+} (100 µM) or 100 µM of other metal ions (black bars) and to the mixture of other metal ions (200 µM) with 100 µM of Cu^{2+} (gray bar portions) in methanol-water (v/v = 7:3, 6 mM HEPES, pH 7.0) solutions.

**Stoichiometries and Affinity Constants of 1-Cu^{2+} Complexes**

In order to understand the binding stochiometry of chemosensor **1**-Cu^{2+}

complexes, Job plot experiments were carried out. Figure 4 plots the emission intensity at 455 nm against molar fraction of chemosensor **1** given a constant total concentration. Maximum emission intensity was reached when the molar fraction was 0.5, corresponding to a 1:1 ratio between chemosensor **1** and Cu^{2+}. This binding ratio (1:1) for **1**-Cu^{2+} complexes was also supported by ESI Mass in which a peak at 412 (m/z) represents the formation of a 1:1 complex. The association constant K_a was evaluated graphically by plotting $1/"F$ against $1/[Cu^{2+}]$ (Figure 5). The data were linearly fit according to the Benesi–Hilderbrand equation. The K_a value, obtained from the slope and intercept of the line, was found to be $2.75*10^3 M^{-1}$.
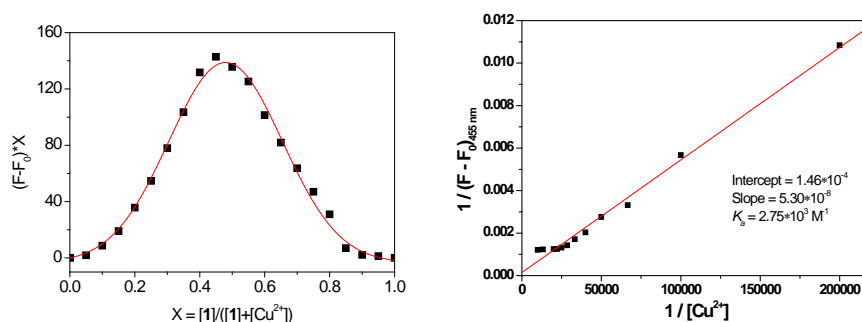
(Left)**Figure 4.** Job plot of the chemosensor **1**-Cu^{2+} complexes in methanol-water (v/v = 7:3, 6 mM HEPES, pH 7.0) solutions. The total concentration ([chemosensor **1**] + [Cu^{2+}]) was 25 μM. (Right) **Figure 5.** Benesi-Hildebrand plot of the chemosensor **1**-Cu^{2+} complexes in methanol-water (v/v = 7:3, 6 mM HEPES, pH 7.0) solutions.
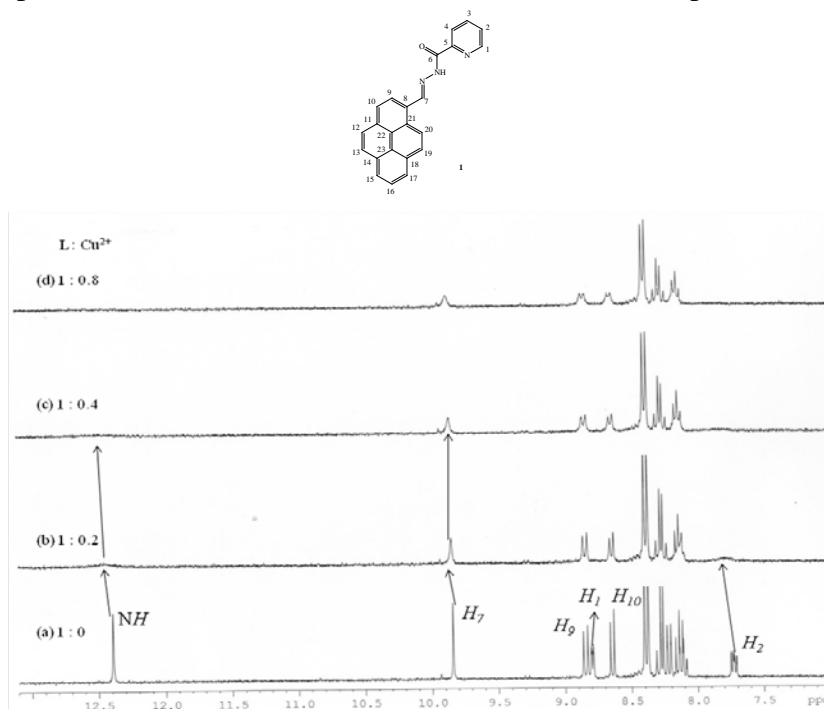
Figure 6. ^{1}H NMR spectra of Chemosensor **1** (5 mM) in the presence of different amount of Cu^{2+} in DMSO-d_6.

To gain a clearer understanding of the structure of chemosensor **1**-Cu^{2+} complexes, ^{1}H NMR and Infrared (IR) spectroscopy were employed. Cu^{2+} is a paramagnetic ion and can affect the proton signals that are close to a Cu^{2+} binding site. In the ^{1}H NMR spectra of chemosensor **1**, adding Cu^{2+} caused the proton (amide NH) signal at 12.4 ppm to almost completely disappear (Figure 6), the proton (at pyridine) signals at 7.6 and 8.8 ppm to disappear, and the intensity of the proton (CH=N) signal at 9.8 ppm to decrease. Other peaks (protons at pyrene) remained unchanged. These observations indicated the binding of Cu^{2+} with an amide group and pyridine. The IR spectra were primarily characterized by bands in the double-bond region. The band 1660 cm^{-1} was associated with double-bond (C=O and C=N) absorption in chemosensor **1**. Binding of Cu^{2+} with chemosensor **1** resulted in a new broad band at 1633 cm^{-1} in the double-bond absorption region, due to the amide group in chemosensor **1**. The Job plot indicates that the binding ratio for chemosensor **1**-Cu^{2+} complexes was 1:1. Cu^{2+} was bound to one nitrogen atom from pyridine and one nitrogen atom from amide (Figure 7).
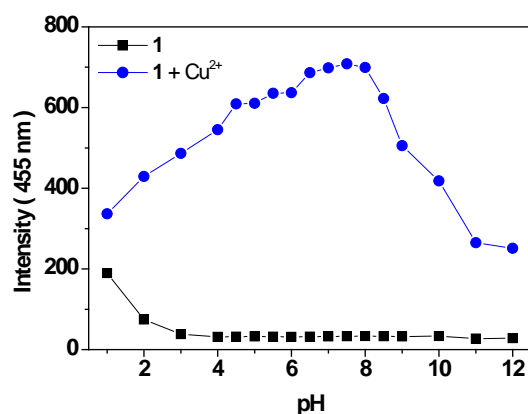

Figure 8. Fluorescence intensity (455 nm) of free chemosensor **1** (25 µM)(black squares) and after addition of Cu^{2+} (100 µM) (blue circles) in methanol-water (v/v = 7:3, 6 mM buffer) solutions as a function of pH. The excitation wavelength was 360 nm.

The study performed pH titration of chemosensor **1** to investigate a suitable pH range for Cu^{2+} sensing. As depicted in Figure 8, the emission intensities of metal-free chemosensor **1** were very low. When pH fell below 2, the emission intensity increased, due to the protonation on the amine in the imine bond. After mixing chemosensor **1** with Cu^{2+}, the emission intensity at 455 nm increased and reached maximum in the pH range of 6 – 8. Above pH 8.0, the emission intensity decreased. This indicates poor stability of the chemosensor **1**-Cu^{2+} complexes at high pH values. At pH < 4, the emission intensity decreased, due to the protonation of the amine groups that prevented the formation of chemosensor **1**-Cu^{2+} complexes.

Live Cell Imaging

    Chemosensor **1** was further applied for live cell imaging. For the detection of Cu^{2+} in live cells, HeLa cells were cultured in DMEM supplemented with 10 % FBS at 37 °C and 5 % CO_2. Cells were plated on 14 mm glass coverslips and allowed to adhere for 24 hours. HeLa cells were treated with 10 μM $CuCl_2$ for 1 hour and washed with PBS for three times. Then cells were incubated with chemosensor **1** (10 μM) for 30 min and washed with PBS to remove the remaining sensor. The images of the HeLa cells were obtained by a fluorescence microscope. Figure 9 shows the images of HeLa cells with chemosensor **1** after the treatment of Cu^{2+}. The overlay of fluorescence and bright-field images reveals that the fluorescence signals are localized in the intracellular area, indicating a subcellular distribution of Cu^{2+} and good cell-membrane permeability of chemosensor **1**.

(a)   (b)   (c)
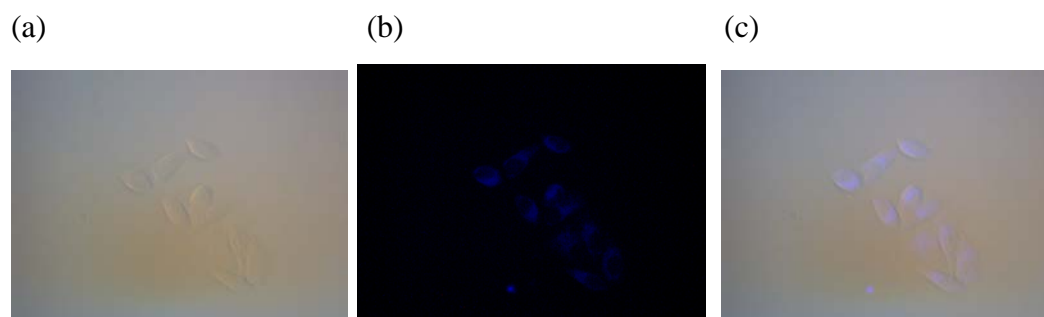
Figure 9. Cu^{2+}-treated HeLa cell images. (a) bright field image; (b) fluorescence image; (c) merged image.

Conclusion

    This study developed a pyrene-based fluorescent chemosensor for Cu^{2+} sensing. The experiment synthesized chemosensor **1** from the reaction of 1-pyrenecarboxaldehyde hydrazone and picolinoyl chloride to form an amide bond. Fluorescence was significantly enhanced with chemosensor **1** in the presence of Cu^{2+}, but adding instead Ag^+, Ca^{2+}, Cd^{2+}, Co^{2+}, Fe^{2+}, Fe^{3+}, Hg^{2+}, K^+, Mg^{2+}, Mn^{2+}, Ni^{2+}, Pb^{2+}, or Zn^{2+} to the chemosensor solution barely affected fluorescence emission. The optimal pH range for Cu^{2+} detection by chemosensor **1** is 5 ~ 8. This pyrene-based Cu^{2+} chemosensor also provides an effective method of Cu^{2+} sensing in live cell imaging.

第五篇論文（*European Journal of Organic Chemistry*, **2012**），合成以bodipy化合物可用來偵測 Hg(II)，當Hg(II)鍵結時會產生綠色螢光，且對Hg(II)具有高度專一性。
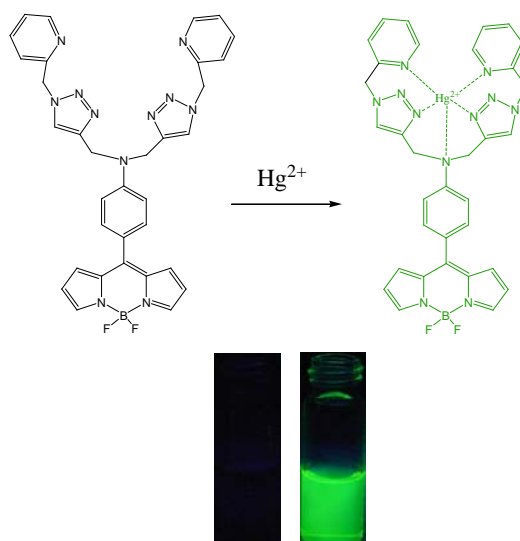

Synthesis of FS1

The synthesis of **FS1** is outlined in scheme 1. Aniline was reacted with propargyl bromide in the presence of K_2CO_3 to afford compound **1**. Compound **2** was obtained by reaction of compound **1** with $POCl_3$ in the presence of DMF at 80 ^{o}C. Treatment of compound **2** with excess pyrrole in presence of TFA under a nitrogen atmosphere yielded corresponding dipyrromethane (compound **3**). In the next step compound **3** was oxidized with DDQ to yield corresponding dipyrromethene, then, transformed to the bodipy skeleton (compound **4**) in presence of BF_3 under N_2 atmosphere. Treatment of compound **4** with picolyl azide yielded **FS1** under click chemistry conditions. **FS1** has an absorbance maxima at 493 nm assigned to the S_0 - S_1 transition of the BODIPY chromophore,[10] with molar extinction coefficient ($\mu = 3.83 \times 10^4$ $M^{-1}cm^{-1}$). **FS1** displayed weak fluorescence, with a quantum yield of ¦ =0.002, since photo-induced electron transfer from the aromatic amine group to the bodipy moiety was taking place.
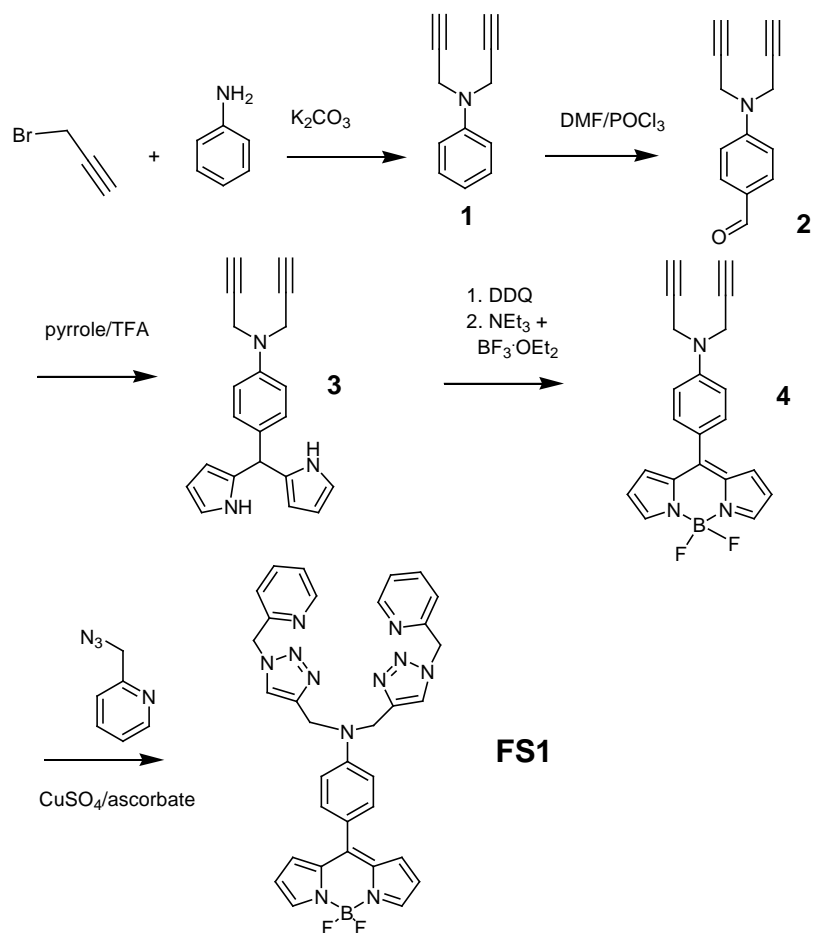
**Scheme 1.** Synthesis of **FS1**

Cation sensing selectivity

The sensing ability of **FS1** was tested by mixing it with metal ions, Ag^+, Ca^{2+}, Cd^{2+}, Co^{2+}, Cu^{2+}, Fe^{2+}, Fe^{3+}, Hg^{2+}, K^+, Mg^{2+}, Mn^{2+}, Ni^{2+}, Pb^{2+} and Zn^{2+}. Qualitatively, Hg^{2+} was the only ion that caused a visible color change (from red to yellow) and green fluorescence from **FS1** (Figure 1). Other metal ions led to no significant change in the fluorescence of **FS1**. Quantitative fluorescence spectra of **FS1** were taken in the presence of several transition metal ions. Hg^{2+} was the only metal ion that caused a significant green emission (Figure 2). During Hg^{2+} titration with **FS1**, a new emission band centered at 520 nm formed (Figure 3). After adding 4 equivalents of Hg^{2+}, the emission intensity reaches a maximum. The quantum yield of the emission band was $\varphi = 0.035$, which is 17-fold higher than that of **FS1**, with $\varphi = 0.002$. These observations indicate that Hg^{2+} is the only metal ion that readily binds with **FS1**, causing significant fluorescence enhancement and permitting highly selective detection of Hg^{2+}.
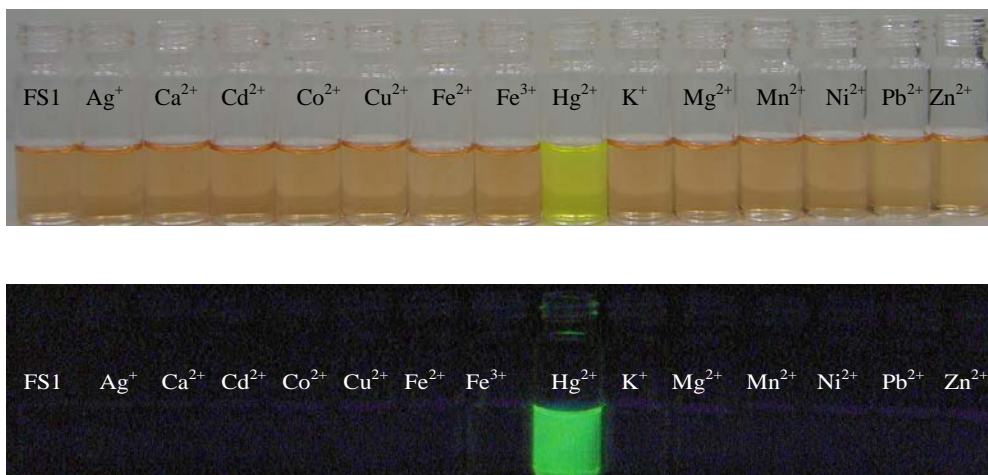
Figure 1. Color (top) and fluorescence (bottom) changes of **FS1** (30 µM) upon the addition of various metal ions (60 µM) in methanol.
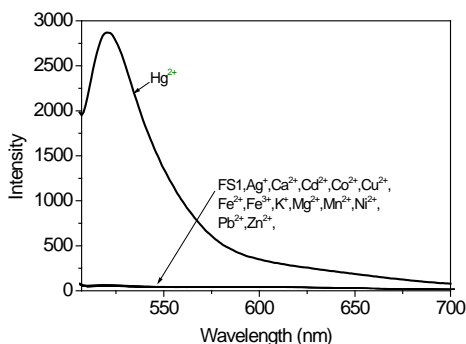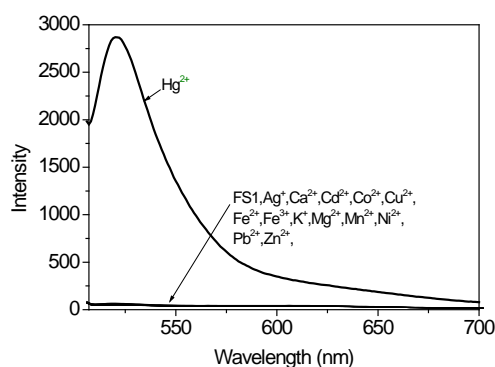

Figure 2. Fluorescence response of **FS1** (30 µM) and other metal cations (30 µM) in methanol. The excitation wavelength was 492 nm.

To study the influence of other metal ions on Hg^{2+} binding with **FS1**, we performed competitive experiments in the presence of Hg^{2+} (150 µM) with other metal ions (150 µM) (Figure 4). Fluorescence enhancement caused by the mixture of Hg^{2+} with most metal ions was similar to that caused by Hg^{2+} alone. A smaller fluorescence enhancement was observed when Hg^{2+} was mixed with Co^{2+} or Fe^{3+}. This indicates that only Co^{2+} and Fe^{3+} compete with Hg^{2+} for binding with **FS1**. Most of the other metal ions do not interfere with the binding of **FS1** with Hg^{2+}.

In order to understand the binding stoichiometry of **FS1**-Hg^{2+} complexes, Job plot experiments were carried out. In Figure 5, the emission intensity at 520 nm was plotted as a function of the mole fraction of **FS1** under a constant total concentration. Maximum emission intensity was reached when the mole fraction was 0.5. These results indicate a 1:1 ratio for **FS1**-Hg^{2+} complexes, in which one Hg^{2+} ion was bound with one **FS1**. Further, the formation of 1:1 **FS1**-Hg^{2+} complex was confirmed using ESI-MS in which the peak at m/z 828.1 indicates a 1:1 stoichiometry for **FS1**-Hg^{2+}

complexes (see Figure S9 in the supplementary data). The apparent dissociation constant was calculated from Figure 4 by using nonlinear regression analysis and was found to be 62.1 ± 5.7 µM (see Figure S10 in the supplementary data).
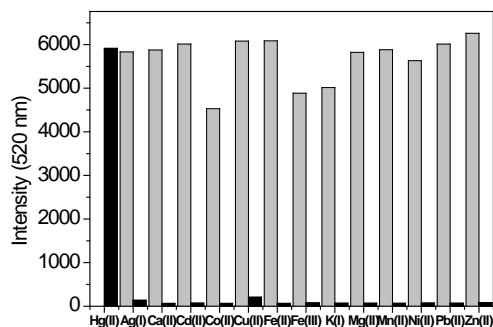

Figure 2. Fluorescence response of **FS1** (30 µM) and other metal cations (30 µM) in methanol. The excitation wavelength was 492 nm.
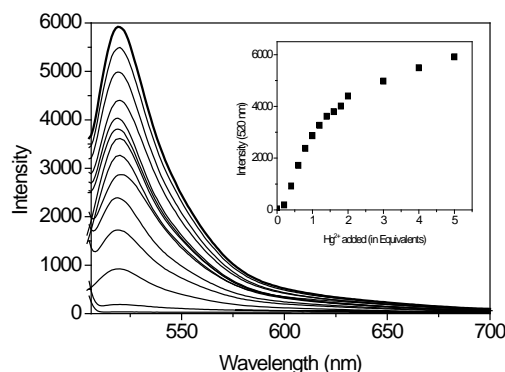


Figure 3. Fluorescence response of **FS1** (30 µM) to various equivalents of Hg^{2+} in methanol. The excitation wavelength was 492 nm.

To gain a clearer understanding of the structure of **FS1**-Hg^{2+} complexes, ^{1}H NMR spectroscopy (Figure 6) was employed. Hg^{2+} is a heavy metal ion and can affect the proton signals that are close to Hg^{2+} binding.[11] In the ^{1}H NMR spectra of **FS1**, the proton (H_g, triazole) signal at 7.8 ppm showed down-field shifts upon the addition of Hg^{2+}. This indicated that Hg^{2+} binding occurs mainly through the nitrogen at the triazole ring. The proton signals (H_e and H_d) showed up-field shifts upon the addition of Hg^{2+}. This also indicated that Hg^{2+} binding was through the amine attached to the phenyl ring. The proton signals (H_i, H_j, H_k & H_l) at the pyridine were slightly influenced by Hg^{2+} binding. These observations reveal that Hg^{2+} binding with **FS1** was through one amine, two nitrogens at two triazole units, and two nitrogens at pyridine moieties.

Figure 4. Fluorescence response of **FS1** (30 µM) to Hg^{2+} (150 µM) or 150 µM of other metal ions (black bars) and to the mixture of other metal ions (150 µM) with 150 µM of Hg^{2+} (gray bars) in methanol.
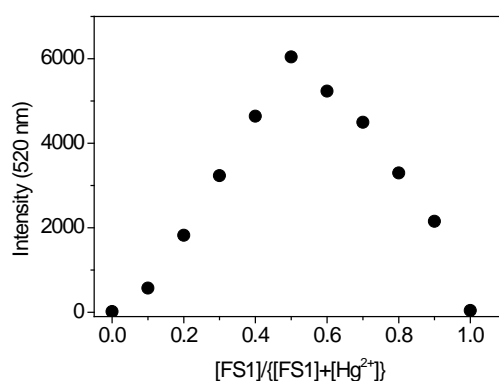
Figure 5. Job plot of Hg^{2+}-**FS1** complexes in methanol. The monitored wavelength was 520 nm. The total concentration of sensor and Hg^{2+} ion was 250 μM.
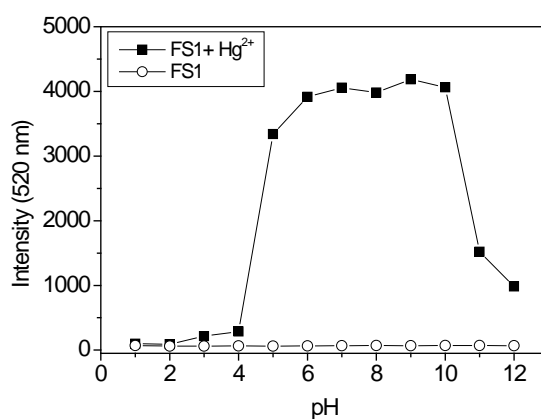
Figure 7. Fluorescence intensity (520 nm) of free **FS1** (30 µM) (Ë) and after addition of Hg^{2+} (150 ¼M) ( ) in a methanol-water (v/v = 9/1, 1 mM HEPES buffer) solution as a function of different pH values. The excitation wavelength was 492 nm.
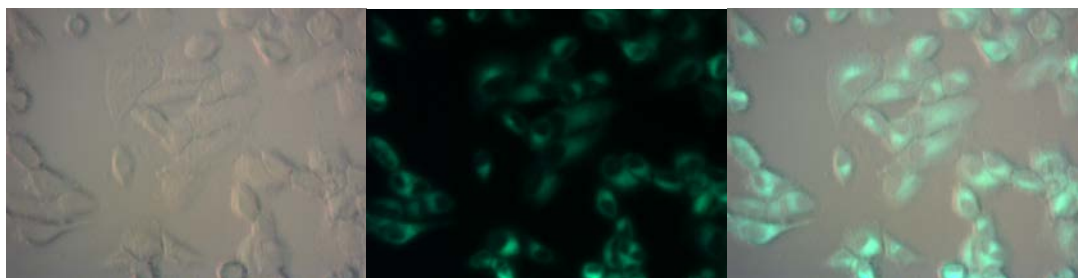
Figure 7. Hg^{2+}-treated HeLa cell images. (a) Bright field image; (b) fluorescence image; and (c) merged image.

Living cell imaging

FS1 was further applied for living cell imaging. For the detection of Hg^{2+} in living cells, HeLa cells were cultured in DMEM supplemented with 10 % FBS at 37 °C and 5 % CO_2. Cells were plated on 14 mm glass coverslips and allowed to adhere for 24 hours. HeLa cells were treated with 10 µM $Hg(BF_4)_2$ for 30 min and washed with PBS for three times. Then cells were incubated with FS1 (10 µM) for 30 min and washed with PBS to remove the remaining sensor. The images of the HeLa cells were obtained using a fluorescence microscope. Figure 7 shows the images of HeLa cells with FS1 after the treatment of Hg^{2+}. The overlay of fluorescence and bright-field images reveal that the fluorescence signals are localized in the intracellular area, indicating a subcellular distribution of Hg^{2+} and good cell-membrane permeability of FS1.

Conclusion:

In summary, the new fluorescence chemosensor FS1 exhibits a high affinity and selectivity for Hg^{2+} ions over competing metal ions. Fluorescence was significantly enhanced by chemosensor FS1 being in the presence of Hg^{2+}, and the addition of Ag^+, Ca^{2+}, Cd^{2+}, Co^{2+}, Cu^{2+}, Fe^{2+}, Fe^{3+}, K^+, Mg^{2+}, Mn^{2+}, Ni^{2+}, Pb^{2+}, or Zn^{2+} barely affected the fluorescence. This BODIPY-based Hg^{2+} chemosensor also provides an effective method of Hg^{2+} sensing in living cell imaging.

第六篇論文（Organic & Biomolecular Chemistry, **2012**），合成以bodipy 化合物可用來偵測 Hg(II)，當Hg(II)鍵結時會產生紅色螢光，且對Hg(II)具有高度專一性。
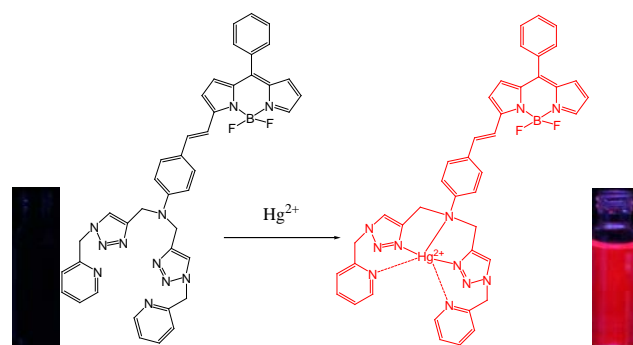
**Synthesis of MS1**
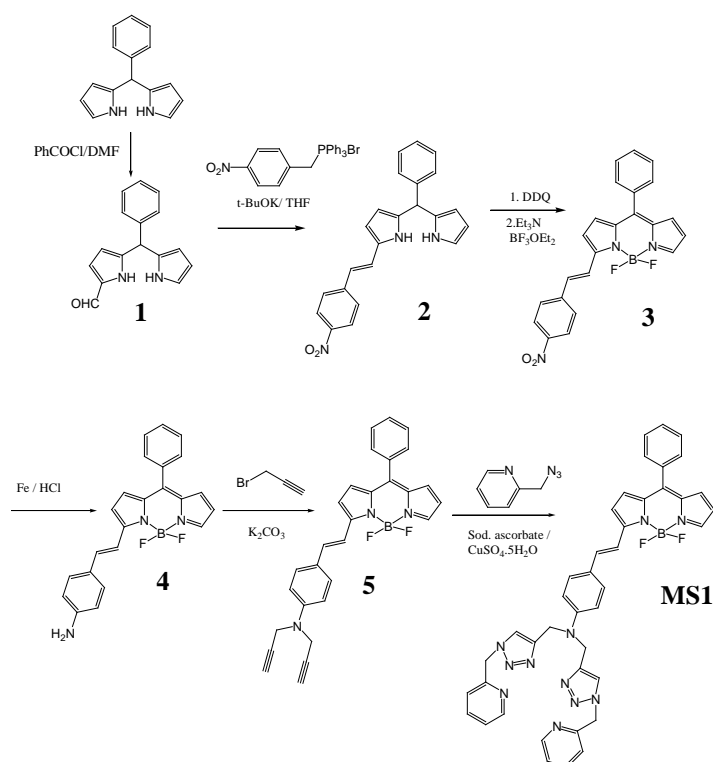

The synthesis of the fluorescent probe, **MS1**, is outlined in Scheme 1. Mono formylated dipyrromethane (1) was synthesized according to the procedure found in the literature[9]. Compound 2 was obtained by a Wittig reaction of (4-nitrobenzyl)triphenyl phosphonium bromide and mono formylated dipyrromethane to form a double bond between pyrrole and nitrobenzene. In the next step, compound 2 was transformed into a BODIPY skeleton by a stepwise reaction; first, dipyrromethane was oxidized to form dipyrromethene by DDQ, followed by dipyrromethene conversion into a BODIPY in the presence of boron trifluoride. Further reduction of compound 3 using iron powder gave compound 4. The reaction of compound 4 with propargyl bromide in the presence of potassium carbonate

yielded compound 5. **MS1** was obtained by treatment of compound 5 with picolyl azide under click chemistry conditions. The absorption spectrum of **MS1** displays an absorption peak centered at 606 nm with a molar extinction coefficient of $6.2 * 10^4$ $M^{-1}cm^{-1}$. The absorption maximum of **MS1** has about a 100 nm red shift in comparison to that of the standard BODIPY dye.[8] This red shift was assigned to a substitution of an amino styryl group at the "3" position of the BODIPY group.
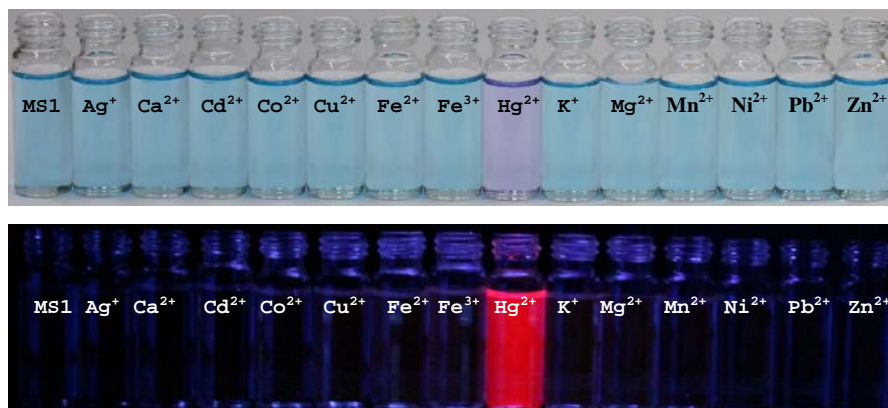
**Figure 1**. Colorimetric change (top) and fluorescence change (bottom) of **MS1** (4 μM) with 60 μM of individual cations.
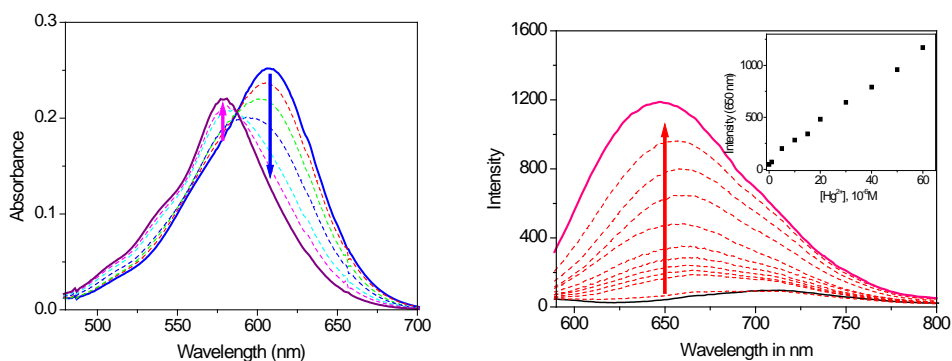
Figure 2. Absorption (left) and emission (right) changes of chemosensor **MS1** (4 μM) in the presence of various equivalents of Hg^{2+} in acetonitrile-water (v/v = 9/1, 2.5 mM Hepes, pH 7.0) solutions.

Cation sensing selectivity

The sensing ability of **MS1** was tested by mixing it with metal ions Ag^+, Ca^{2+}, Cd^{2+}, Co^{2+}, Cu^{2+}, Fe^{2+}, Fe^{3+}, Hg^{2+}, K^+, Mg^{2+}, Mn^{2+}, Ni^{2+}, Pb^{2+}, and Zn^{2+}. Qualitatively, Hg^{2+} was the only ion that caused a visible color change (from blue to purple) and red fluorescence from **MS1** (Fig. 1). Other metal ions led to no significant change in the fluorescence of **MS1**. Quantitative absorption and fluorescence spectra of **MS1** were taken in the presence of several transition metal ions. Hg^{2+} was the only metal ion that caused a significant red emission (Fig. 2). During Hg^{2+} titration with **MS1**, the absorption band at 606 nm was shifted to 577 nm (Fig. 2). This caused a visible color

change from blue to purple. During Hg^{2+} titration with **MS1**, a new emission band centered at 650 nm formed (Fig. 2). After adding 15 equivalents of Hg^{2+}, the quantum yield of the emission band was ǀ = 0.327, which is 65 fold higher than that of **MS1**, with ǀ = 0.005. These observations indicate that Hg^{2+} is the only metal ion that readily binds with **MS1**, causing significant fluorescence enhancement and permitting highly selective detection of Hg^{2+}.
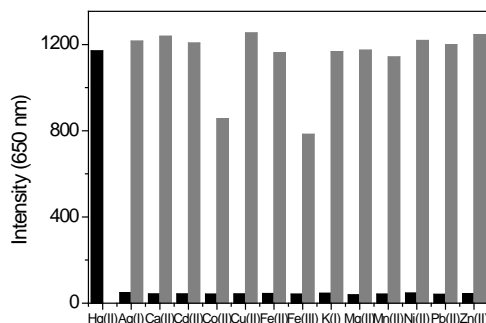
Figure 3. Fluorescence response of **MS1** (4 µM): to the addition of Hg^{2+} (60 µM); or 150 µM of other metal ions (black bars) and to the mixture of other metal ions (150 µM) with 60 µM of Hg^{2+} (gray bars) in acetonitrile-water (v/v = 9/1, 2.5 mM Hepes, pH 7.0) solutions. The excitation wavelength is 550 nm.
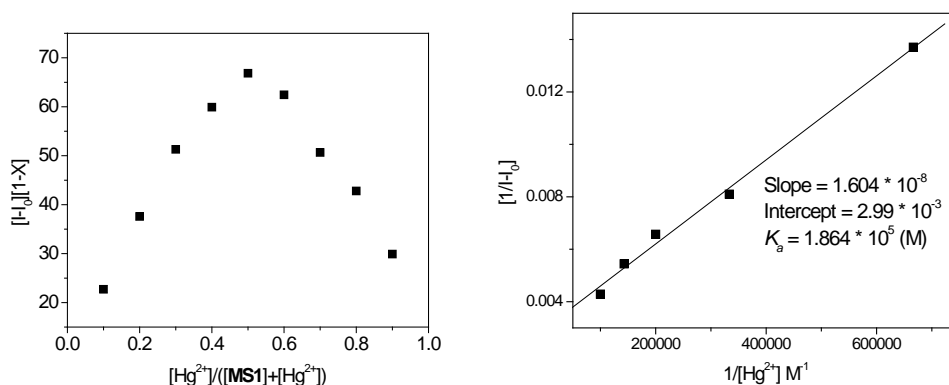

(Left) **Figure 4**. Job plot of Hg^{2+}-**MS1** complexes in acetonitrile-water (v/v = 9/1, 2.5 mM Hepes, pH 7.0) solutions. The monitored wavelength was 650 nm. The total concentration of the sensor and Hg^{2+} ion was 8 µM. (Right) **Figure 5**. Benesi-Hildebrand plot of the Hg^{2+}-**MS1** complexes in in acetonitrile-water (v/v = 9/1, 2.5 mM Hepes, pH 7.0) solutions. The monitored emission wavelength was 650 nm.

To study the influence of other metal ions on Hg^{2+} binding with **MS1**, we performed competitive experiments in the presence of Hg^{2+} (60 µM) with other metal ions (150 µM) (Fig. 3). Fluorescence enhancement caused by the mixture of Hg^{2+} with most metal ions was similar to that caused by Hg^{2+} alone. A smaller fluorescence enhancement was observed when Hg^{2+} was mixed with Co^{2+} or Fe^{3+}. This indicates that only Co^{2+} and Fe^{3+} compete with Hg^{2+} for binding with **MS1**. Most of the other

metal ions do not interfere with the binding of **MS1** with Hg^{2+}.

In order to understand the binding stoichiometry of **MS1**-Hg^{2+} complexes, Job plot experiments were carried out. In Fig. 4, the emission intensity at 650 nm was plotted as a function of the mole fraction of **MS1** under a constant total concentration. Maximum emission intensity was reached when the mole fraction was 0.5. These results indicate a 1:1 ratio for **MS1**-Hg^{2+} complexes, in which one Hg^{2+} ion was bound with one **MS1**. Further, the formation of 1:1 **MS1**-Hg^{2+} complex was confirmed using ESI-MS in which the peak at m/z 929.9 indicates a 1:1 stoichiometry for **MS1**-Hg^{2+} complexes (see Figure S11 in the supplementary data). The apparent association constant was calculated from Fig. 5 by using nonlinear regression analysis and was found to be $1.864*10^5$ M^{-1}. The detection limit of **MS1** as a fluorescent sensor for the analysis of Hg^{2+} was determined from the variation of fluorescence intensity as a function of the concentration of Hg^{2+} (see Figure S12 in the supplementary data). It was found that **MS1** has a detection limit of 0.226 μm, which allows micromolar concentrations of Hg^{2+} to be detected.
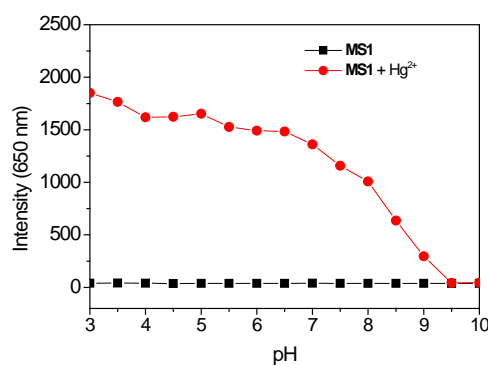

Figure 6. Fluorescence intensity (650 nm) of **MS1** (4 ¼M) ( ), and after addition of Hg^{2+} (60 μM) (Ï) in an acetonitrile:water (v/v= 9:1, 2.5 mM buffer) solution as a function of different pH values. The excitation wavelength was 550 nm.

A pH titration of **MS1** was performed to investigate a suitable pH range for Hg^{2+} sensing. As depicted in Fig. 6, the emission intensities of metal-free **MS1** were very low. After mixing **MS1** with Hg^{2+}, the emission intensity at 650 nm remained a maximum in the pH range of 3.0 ~ 7.0. Above pH 7.5, the emission intensity decreased. This indicates poor stability of the **MS1**-Hg^{2+} complexes at high pH values.

To gain a clearer understanding of the structure of **MS1**-Hg^{2+} complexes, ^1H NMR spectroscopy (Fig. 7) was employed. Hg^{2+} is a heavy metal ion and can affect the proton signals that are close to Hg^{2+} binding.[9] In the ^1H NMR spectra of **MS1**, the proton (H_l, triazole) signal at 7.75 ppm showed down-field shifts upon the addition of Hg^{2+}. The down-field shifts upon Hg^{2+} coordination are due to a decrease in electron

density induced by Hg^{2+}. This indicated that Hg^{2+} binding occurs mainly through the nitrogen at the triazole ring. The proton signals (H_j and H_k) showed up-field shifts upon the addition of Hg^{2+}. This indicated that Hg^{2+} binds to the amine attached to the phenyl ring and Hg^{2+} binding affects the ring current in the phenyl ring. The proton signals (H_n, H_o, H_p & H_q) at the pyridine were slightly influenced by Hg^{2+} binding. This showed weak interactions between Hg (II) and the pyridines. These observations revealed that Hg^{2+} binding with **MS1** was mainly through one amine, two nitrogens at two triazole units and Hg^{2+} had weak interactions with two nitrogens at pyridine moieties.
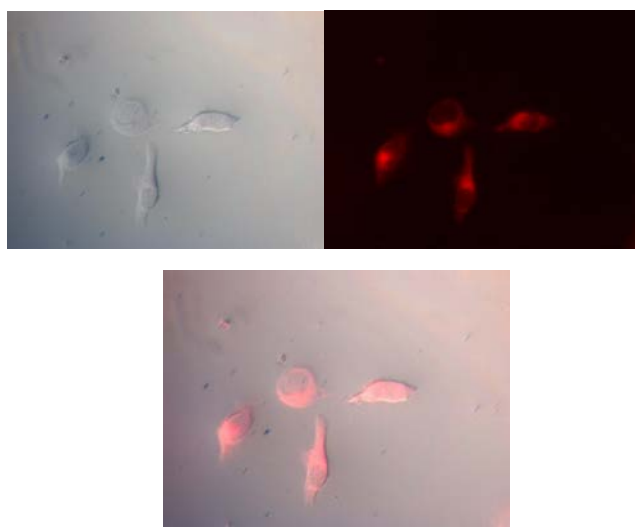
Figure 8. Hg^{2+}-treated HeLa cell images. (Top left) Bright field image; (Top right) fluorescence image; and (Bottom) merged image.

Living cell imaging

   MS1 was also applied to living cell imaging. For the detection of Hg^{2+} in living cells, HeLa cells were cultured in DMEM supplemented with 10 % FBS at 37 °C and 5 % CO_2. Cells were plated on 14 mm glass coverslips and allowed to adhere for 24 hours. HeLa cells were treated with 20 µM $Hg(BF_4)_2$ for 30 min and washed with PBS for three times. Then cells were incubated with **MS1** (20 µM) for 30 min and washed with PBS to remove the remaining sensor. The images of the HeLa cells were obtained using a fluorescence microscope. Fig. 8 shows the images of HeLa cells with **MS1** after the treatment of Hg^{2+}. The overlay of fluorescence and bright-field images reveal that the fluorescence signals are localized in the intracellular area, indicating a subcellular distribution of Hg^{2+} and good cell-membrane permeability of **MS1**.

Conclusions

   In summary, the new fluorescence chemosensor **MS1** exhibits a high affinity and selectivity for Hg^{2+} ions over competing metal ions. Fluorescence was significantly

enhanced by chemosensor **MS1** being in the presence of Hg^{2+}, and the addition of Ag^+, Ca^{2+}, Cd^{2+}, Co^{2+}, Cu^{2+}, Fe^{2+}, Fe^{3+}, K^+, Mg^{2+}, Mn^{2+}, Ni^{2+}, Pb^{2+}, or Zn^{2+} barely affected the fluorescence. This BODIPY-based Hg^{2+} chemosensor also provides an effective method of Hg^{2+} sensing in living cell imaging.